Available online at www.sciencedirect.com
SCIENCE DIRECT
Polymer 47 (2006) 330–340
polymer
www.elsevier.com/locate/polymer

Crystallization of block copolymers in restricted cylindrical geometries

Cvetelin Vasilev [a,*], Günter Reiter [a], Stergios Pispas [b,1], Nikos Hadjichristidis [b]

[a] *Institut de Chimie des Surfaces et Interfaces, CNRS-UHA, 15, rue Jean Starcky, B.P. 2488, 68057 Mulhouse cedex, France*
[b] *Department of Chemistry, University of Athens, Panepistimiopolis Zografou, 157 71 Athens, Greece*

Received 2 August 2004; received in revised form 14 July 2005; accepted 10 November 2005
Available online 29 November 2005

Abstract

Using Tapping Mode atomic force microscopy, we studied crystallization of polymers in confined cylindrical geometries of micro-phase separated asymmetric diblock copolymers, deposited in thin films onto solid substrates. We observed that in most cases crystallization occurs separately and independently in each cylinder of the mesophase pattern. We followed the kinetics of the crystallization process with time and found an influence of the lateral size of the cylindrical morphology on the rate of crystallization. The present data are compared to previous results on spherical mesophase patterns. The growth rate within one single cylinder was found to be not necessarily constant. Depending on the amount of crystallized material and the molecular weight, structural relaxations of the crystals can have very strong influence on the amorphous matrix and can even lead to the destruction of the mesophase pattern, allowing for break-out crystallization. As a consequence of break-out crystallization, crystallization kinetics changed considerably since the crystal growth was not limited anymore to the confinement imposed by the cylinders.

Keywords: Atomic force microscopy; Confined crystallization; Block copolymers

1. Introduction

Recently, the morphology of crystalline/amorphous block copolymers and morphology changes upon crystallisation have attracted considerable attention. Studies on these materials have the potential to shed light on the fundamental physics of polymer crystallization as well as on crystallization in confined geometry. The processes of nucleation and crystal growth can get more complex by lateral confinement of the crystallisable block resulting from self-organization in nanometer-sized phase separated domains [1–15]. Many diblock copolymer systems with one crystallisable block, including poly(ethylene) [16–24], poly(ethylene oxide) (PEO) [25–31], poly(caprolactone) [32] and poly(tetrahydrofuran) [33,34] have been studied. The corresponding amorphous blocks vary considerably in terms of their glass transition temperatures and their interaction parameter with the crystallisable block. The first studies on polystyrene–poly(ethylene oxide) diblock copolymers were done by Lotz and Kovacs [35,36], where the crystalline structure of PEO in solution grown diblock copolymer single crystals was investigated. Hamley, Ryan, and co-workers recently studied the morphology and crystallization kinetics of a series of poly(ethylene oxide-*b*-butylene oxide) and poly(ethylene oxide-*b*-propylene oxide) diblock copolymers [18,27,37].

In many of these previous studies on diblock and triblock copolymers, crystallization was studied by DSC and X-ray techniques in bulk samples. It was found that the final morphology was path-dependent [38–46]. When crystallizing the sample from a microphase-separated melt state, two kinds of results were obtained: 1. The microphase-separated morphology was maintained, and the crystallisable block crystallized within the volume defined by this morphology. 2. Crystallization destroyed the microphase-separated morphology, and a spherulitic texture was formed. In addition, similar to crystallisable homopolymers, the resulting morphology was found to be heavily influenced by the crystallization kinetics. Diblock copolymers with one crystallisable block exhibit characteristics of both, simple crystalline homopolymers and microphase separated amorphous diblock copolymers. Thermodynamically, two opposing driving forces compete for determining the final morphological structure in the crystalline state. If the system is sufficiently strongly phase-separated in the melt, crystallization may be confined within

* Corresponding author. Present address: Physics and Astronomy Department, University of Sheffield, Hounsfield Road, Sheffield S3 7RH, UK. Tel.: +44 114 222 4357; fax: +44 114 272 8079.
E-mail address: c.vasilev@sheffield.ac.uk (C. Vasilev).
[1] Present address: Theoretical and Physical Chemistry Institute, National Hellenic Research Foundation, 48 Vas. Constantinou Ave., 11635 Athens, Greece.

0032-3861/$ - see front matter © 2005 Elsevier Ltd. All rights reserved.
doi:10.1016/j.polymer.2005.11.040

the microdomains existing already in the melt. In such cases, the melt morphology is preserved on cooling, i.e. we are dealing with templated crystallization. However, if crystallization is the stronger driving force, the melt morphology can be disrupted on cooling and we observe spherulite formation. In this case, we are dealing with break-out crystallization.

Although a relatively large amount of work exists on crystallisable block copolymers in the bulk, much less work has been done in thin films [37].

In the here presented experiments, we used atomic force microscopy (AFM) to study crystallization of semi-crystalline block copolymers in thin (60–80 nm) films. In particular, we studied in situ the average kinetics of the crystallization process in confined cylindrical geometries formed in microphase separated highly asymmetric block copolymers. Studies on systems where the crystallisable block was confined in spherical nano-domains [38] or systems where the crystallisable polymer is confined in droplets with diameter of few micrometers [39] down to 100 nm [40] showed that homogeneous nucleation was at work in such systems and was only possible at large undercoolings. In such cases, the resulting crystals were each restricted to a single mesophase domain. All crystals were formed independently without any visible coupling between neighbouring domains. Crystallization at large undercoolings results in a variety of metastable crystals which contained many defects and thus, they are quite imperfect and show a tendency to improve their crystalline order. Here, we are aiming at studying the corresponding relaxation processes within the crystals and the surrounding amorphous material upon annealing above the crystallization temperature, but always staying well below the melting temperature. The key question obviously is if these relaxation processes can be detected by AFM at room temperature, for example via changes in the characteristic spacing or in the geometry of the mesophase pattern. We want to study whether the block copolymer microphase structure, with a length scale of a few tens of nanometers, could be used to template crystallization, even when the matrix polymer remains above its glass transition temperature and thus stays liquid-like. To this end, we will determine in detail under which conditions the growth front will follow the mesophase pattern. Taking into account kinetic effects, we examine when break-out crystallization is faster or slower than templated crystallization. In this context, in order to prevent the possibility of break-out crystallization, we cross-linked the amorphous surrounding of the crystalline cells. Another crucial question concerns nucleation in such confined geometries. As in similar systems of nanometer confinement, we expect homogeneous nucleation, because the number of separate compartments in the mesophase is much higher then the number of defects and impurities, which are present in the sample. Thus, most of the compartments are free of defects, which could potentially induce heterogeneous nucleation. However, in cylinders, one may also expect that the crystals once nucleated continue to grow along the cylinder. But it is unclear if this is the case and if so, if the crystal growth rate is constant or not.

2. Experimental

In this work, we used the following polymers.

A poly(ethylene-*co*-butylene)-*block*-poly(ethylene oxide) (PEB-*b*-PEO), with a molecular weight of the blocks of 3700 and 1400 g/mol, respectively, corresponding to a PEO weight fraction of 28%. The polymer was obtained from the group of Professor G. Riess, ENSCMu, Mulhouse, France. In the following, this system is designated as BEO 28. It forms microphase separated structures consisting of cylindrical domains of the minority block (PEO) of a diameter of 8 nm embedded in a matrix formed by the majority block (PEB).

The second polymer was non-hydrogenated poly(butadiene-*block*-ethylene oxide) (PB-*b*-PEO), with a molecular weight of the blocks of 23,500 and 7800 g/mol, respectively, corresponding to a PEO weight fraction of 25%, a polydispersity of 1.07, and designated as BEO 25. This highly asymmetric diblock copolymer also forms microphase structures consisting of cylindrical domains (18 nm in diameter) of the minority block (PEO) embedded in a matrix formed by the majority block (PB).

The two systems have melting temperatures in the range from 45 to 55 °C, depending on the crystallization temperature and the thermal history of the sample after the crystallization. The microstructure of the glassy block of the BEO 25 system consists of statistically distributed 1,2 and 1,4 butadiene units with majority of the 1,2 units (about 80%) which determines a glass transition temperature of about −20 °C. For the BEO 28 the fraction of the 1,4 units is higher (probably about 40%), hence the glass transition temperature is lower—about −40 °C. Thin polymer films with a thickness of about 80 nm were spin-coated on UV–ozone cleaned Si substrates from dilute toluene solution (concentration about 20 mg/ml). The spin-coating was conducted at 2000 min^{-1} by a PWM32-R790 spincoater form Headway Research, TX, USA. Reproducible starting conditions of well-ordered microphase structures were obtained by annealing the films at 160 °C for about 20 min, employing heating and cooling rates of typically 10 °C/min, realized in a Linkam THMS 600 hot-stage with TMS 91 controller. The thickness and the annealing conditions were the same for each system, BEO 28 and BEO 25, respectively. A series of identical samples was prepared by cutting a big master sample into smaller pieces. All samples were crystallized under well controlled conditions in the closed chamber of a differential scanning calorimeter (DSC, Mettler-Toledo DSC30) for different periods of time ranging from 2 to 120 min. BEO 28 samples were crystallized at −17 °C and BEO 25 samples at −19 °C, respectively. During crystallization, the DSC chamber was purged with a flow of dry nitrogen. In addition, the cooling and heating rates and the temperature of crystallization were the same for all samples of one series. Only the time of crystallization was varied.

After crystallization, all samples were brought back to room temperature and measured by tapping-mode atomic force microscopy (TM-AFM) at ambient conditions. For all TM-AFM measurements we used a digital instruments multimode AFM (NanoScope IV controller). We used commercial silicon TM-AFM tips (type NCL-W) with a free resonance

frequency in the range from 172 to 191 kHz and spring constants in the range from 33 to 47 N/m. All measurements were done in air.

In order to minimize the influence of possible relaxation processes or crystal growth at room temperature we took precautions to limit the time, which the samples spent at room temperature outside the DSC after the crystallization. Each sample was measured by AFM immediately after crystallization. Typically, we took 5–7 images per sample (size of the images was $2\times2\ \mu m^2$) and the whole procedure (from the removal of the sample from the DSC till the last image) lasted about 30–40 min per sample. Then, each of the measured phase images was converted to binary black and white image. Afterwards, a threshold between black and white was chosen in a such way that the brightest objects on the image, which represent the crystalline PEO domains, became white and all darker objects—molten PEO domains and the amorphous PB matrix, became black. The percentage of the black pixels was counted. On the AFM phase images of fully amorphous BEO 25 samples (0% of crystalline material, there the darkest objects are the amorphous PEO domains) the observed percentage of the black pixels was about $65\pm10\%$, the rest $35\pm10\%$ corresponds to the PB matrix. In case of BEO 28, these values were $70\pm10\%$ and $30\pm10\%$ for the PEO and PB domains, respectively. This implies that on a 100% crystalline sample only about $65–70\pm10\%$ of the surface appeared as bright (i.e. stiff) objects. Consequently, after subtracting the contribution coming from the PB matrix, the area of black pixels defined the amount of non-crystalline PEO. The major error in this method arises from the difficulty to set the threshold in a correct and reproducible way for each image. The relative error could reach 15% and more for the samples with very low content of crystallized material. In addition, sometimes low contrast of the phase images, which could be caused by AFM tips having a comparatively large radius of curvature, complicated also the analysis.

In order to cross-link the PB matrix of the BEO 25 sample, we used 1,1′-azobis(cyclohexanecarbonitrile) free radical initiator (FRI). This initiator decomposes at elevated temperatures with first-order kinetics, it is not sensitive to metals, acids, and bases, and it is not susceptible to radical-induced decompositions. In this work, we used a relatively high cross-linking density (about 1 cross-linking bond per 50 monomers). The initiator was added in the solution before the samples were spin-coated and the concentration was about 1% of the weight of the polymer in the solution. The cross-linking process took place during the annealing of the sample (after the casting from the solution with the FRI in it) at 160 °C (the FRI we used starts to decompose at about 120 °C).

3. Results and discussion

Previous nucleation and crystallization studies on similar systems under confinement in spherical domains [47–54] showed that the number density of microdomains by far exceeds the typical impurity density. Thus, homogeneous nucleation, a phenomenon usually not observed in bulk semi-crystalline homopolymers, is responsible for initiating crystallization in the nanoscale domains of the semi-crystalline block copolymer. A large energy barrier is associated with the formation of a nucleus during the homogeneous nucleation. The rate of homogeneous nucleation J (number of nuclei n formed per unit time and unit volume) at a certain temperature of crystallization T_c, depends in an exponential fashion on the undercooling ΔT_c, i.e. the difference between the temperature of melting T_m and T_c [55]:

$$J = N_0 \exp\left[\frac{-(E_D + \Delta G)}{RT}\right], \tag{1}$$

where $\Delta G \propto 1/\Delta T_c^2$ is the free energy barrier of nucleation, N_0 is the number of molecules per unit volume of the polymer and E_D is a transport term, related to diffusion of the polymer chains to the growth front. The large number of nuclei that is required for independent crystallization of every cell causes that significant crystallization in such nanostructered materials happens only at large undercoolings of about 60–80 K. In analogy to the results observed for spherical compartments [47], we expect a similar nucleation behaviour at large undercoolings also for cylindrical nanoscale confinement.

3.1. Sample morphology

The equilibrium morphological structure of block copolymers is determined by several factors: the extent of 'dislike' between blocks (expressed by the Flory–Huggins interaction parameter, χ), the total chain length N (or molecular weight M_w) and weight fraction of the minority block f (or composition of the system). In an amorphous sample with $f=0.5$, the characteristic spacing d of the mesophase pattern (in the strong segregation limit, $\chi N \gg 10$) is given by [56]:

$$d \propto aN^{2/3}\chi^{1/6}, \tag{2}$$

where a is the characteristic segment length. Polyethyleneoxide (PEO) and polybutadiene (PB) blocks are highly incompatible, also expressed by temperatures for the order–disorder transition far above 200 °C. This results in phase separation, which in the systems we used led to formation of cylindrical domains of crystallisable PEO (Fig. 1). This

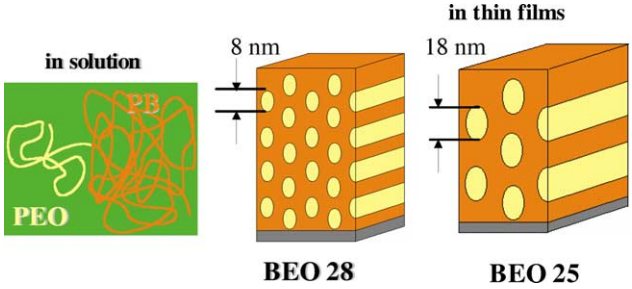

Fig. 1. Morphologies of the used PB–PEO systems: randomly coiled single chains in solution and cylindrical phase separated domains in thin films. The weight fraction of polyethylene oxide is 28 and 25% for BEO 28 and BEO 25, respectively. The diameter of the cylinders (8 and 18 nm) depends on the molecular weight of the PEO block, i.e. 1400 and 7800 g/mol for BEO 28 and BEO 25, respectively.

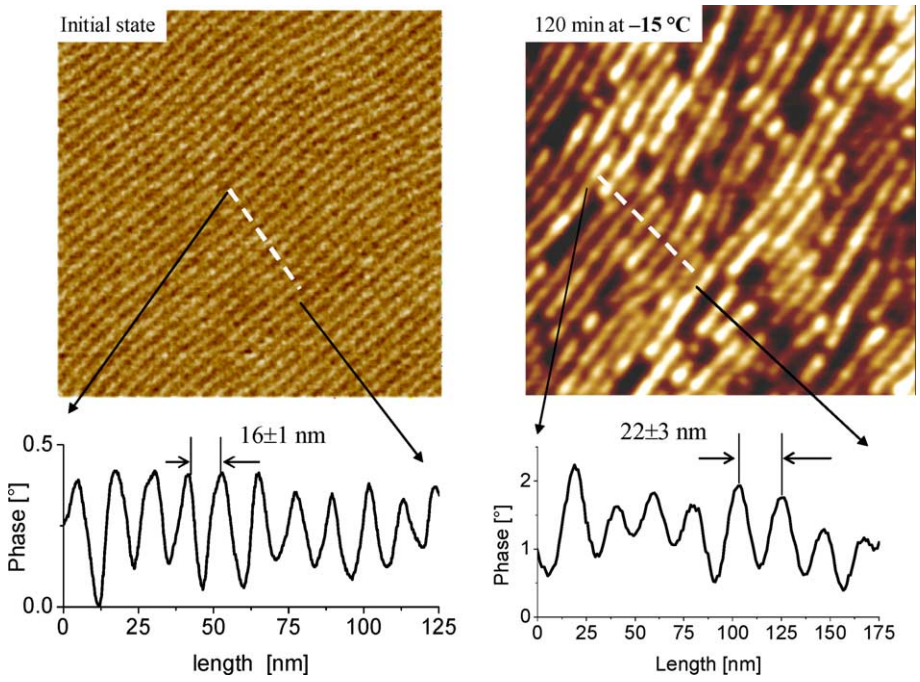

Fig. 2. AFM phase images of BEO 28, size is 500×500 nm^2. On the left-hand side is the initial (amorphous) state and on the right-hand side is the sample after crystallization for 120 min at −15 °C. The corresponding cross-sections give a spacing of 16±1 nm (11 periods per 175 nm) and 22±3 nm (8 periods per 175 nm) for the amorphous and crystalline state, respectively.

organization of the polymers resulted in a pattern observable on the sample surface (by AFM for instance) as a sequence of zones with different mechanical properties. The difference in the surface tension of the different polymer blocks can lead to an organization on the interface polymer/air quite different from the organization of the blocks (phase separation pattern) in bulk sample. In the system we used, the PB block had the lower surface tension (with respect to surface tension of the PEO block) and therefore formed a few nanometers thick surface layer [57,58].

Generally, during crystallization the conformation of the PEO chain changes from a coiled state (with high conformational entropy) to a more ordered state, which even may consist of fully extended chains and hence, with lower conformational entropy. The unfolding of the PEO chains may be accompanied by a stretching of the PB chains (if the PEO chains are often folded, no stretching of the PB chains may be caused). These rearrangements of the PEO and PB chains during the crystallization process can certainly lead to changes in the envelope volume, i.e. the volume occupied by a given number of chains. In particular the form of the envelope may get deformed. In addition, in the crystalline state the density of PEO is higher, thus the volume occupied by the chains should be smaller. All these effects together may lead to changes in the average spacing of the mesophase pattern.

In order to verify if any changes in the arrangement of the PEO chains within the cylinders occur during the transition from the amorphous to the crystalline state, we compared the average characteristic spacing d of the mesophase pattern of the amorphous sample to the average spacing of the crystalline one. We measured by AFM three different samples-BEO 28, BEO 25 and cross-linked BEO 25 after annealing in the amorphous state. BEO 28 samples were then crystallized for 120 min at −15 °C while BEO 25 samples (non-cross-linked and cross-linked) were crystallized for 100 min at −19 °C. After crystallisation, these samples were measured at room temperature by AFM. We compared the average spacing between cylinders. It is important to notice that on the AFM phase images of the still amorphous BEO 28 the brighter lines correspond to the PEO domains and the darker lines correspond to the PB domains (Fig. 2, left-hand side panel). On the phase images of crystallized samples the brighter lines correspond to the crystalline PEO domains, the darker ones are the amorphous PEO domains and the darkest ones represent the PB matrix (Fig. 2, right-hand side panel). We made a cross-section of the AFM phase image in the direction normal to the predominant orientation of the cylindrical microdomains and measured the period directly from the cross-sectional curve, which represents the spacing of the surface pattern of the sample. We obtained 16±1 nm for the spacing of amorphous BEO 28 (coiled state) and 22±3 nm (Fig. 2) for the crystalline state. The error bars were estimated from the maximum deviation of the measured data from the mean value, averaged over all measurements.

On the AFM phase images of amorphous BEO 25 (both cross-linked and non-cross-linked) the phase contrast is inverted with respect to the amorphous BEO 28—where the brighter lines correspond to the PB matrix and the darker ones correspond to the PEO domains (Fig. 3, left-hand side panel). On the phase images of partially crystallized BEO 25 sample the brightest lines correspond to the crystalline PEO domains, the darker ones represent the PB matrix and the darkest ones

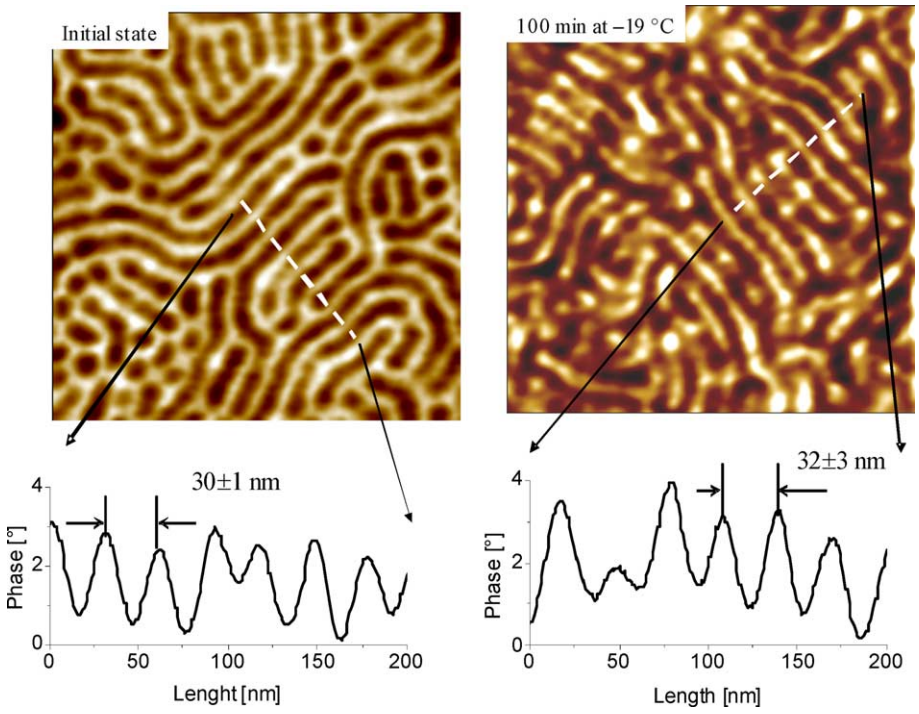

Fig. 3. AFM phase images of BEO 25, size is 500×500 nm^2. On the left-hand side is the initial (amorphous) state and on the right-hand side is the sample after crystallization for 100 min at −19 °C. The corresponding cross-sections give a spacing of 30±1 nm (6 periods per 180 nm) and 32±3 nm (7 periods per 220 nm) for the amorphous and crystalline state, respectively.

are the amorphous PEO domains (Fig. 3, right-hand side panel). A possible explanation of this inversion could be some diminutive difference in the surface energy of the hydrogenated polybutadiene compared to the non-hydrogenated one and thus, different tip-sample interaction over the PB domains for BEO 28 and BEO 25, respectively.

For BEO 25, we measured periods of 30±1 nm in the amorphous (coiled) state and about 32±3 nm in the crystalline state, for both cross-linked (Fig. 3) and non-cross-linked samples. These averaged values were obtained from 5 to 7 measurements per image and 7–10 images per sample. Thus, within the errors, for BEO25 we did not detect a significant change of d caused by crystallisation. In the course of the crystallization process, the crystallisable chains have a tendency to increase their degree of internal order by unfolding (in order to minimize the fold surface energy). On the other hand, there is an entropic penalty of the stretching amorphous chains. The interplay between these two driving forces could in principle lead to an equilibrium state if these two forces were balanced. Such an equilibrium state may, however, contain folded chains. On the way towards such an equilibrium state, the kinetics of the crystallisation process may govern the process of chain unfolding and may cause various non-equilibrium intermediate states, which differ in the degree of perfection of the formed polymer crystals. In addition, the development of closest packing of the crystalline stems within the crystal may be affected or even hindered by the geometry of the PEO mesophase domain. Domain size and shape are predefined by the microphase separation and may be incommensurate with crystal size and shape and thus may not always allow the formation of fully extended PEO chains. In part, the observed large error bars for the spacing measured for the crystalline samples may be due to the different degrees of perfection (i.e. degree of chain folding) of the crystals formed along the cylinder.

We calculated the length of a fully extended PEO block for BEO 28 (M_w (PEO)=1400 g/mol; M_w (PB)=3700 g/mol) and BEO 25 (M_w (PEO)=7800 g/mol; M_w (PB) =23,500 g/mol) to be about 9 nm and about 55 nm, respectively. Comparing these values to the measured spacings, we can conclude that for BEO 28 the PEO blocks are in the most stable crystalline state (lowest free energy of the stems) of fully extended and interdigitating chains. For the width of the BEO 28 crystals at room temperature we measured 10±2 nm (without taking into account the possible tip convolution [59]), which is comparable to the length of fully extended PEO chains. For non-cross-linked and cross-linked BEO 25 we can conclude that within the cylindrical confinement imposed by microphase separation the PEO block can at best form twice folded, interdigitated states. However, at high growth rates, caused by the large undercoolings, more folded, less perfect, metastable states are possible. The width of the PEO crystals at room temperature was measured to be 20±2 nm (again without taking into account the possible tip convolution), which can be compared to 1/2 (=28 nm) or 1/3 (=18 nm) of the length of fully extended PEO chains.

3.2. Relaxation at room temperature

As mentioned already, due to the large undercoolings only highly imperfect crystals were formed. The consequential tendency to increase the internal degree of order of the PEO

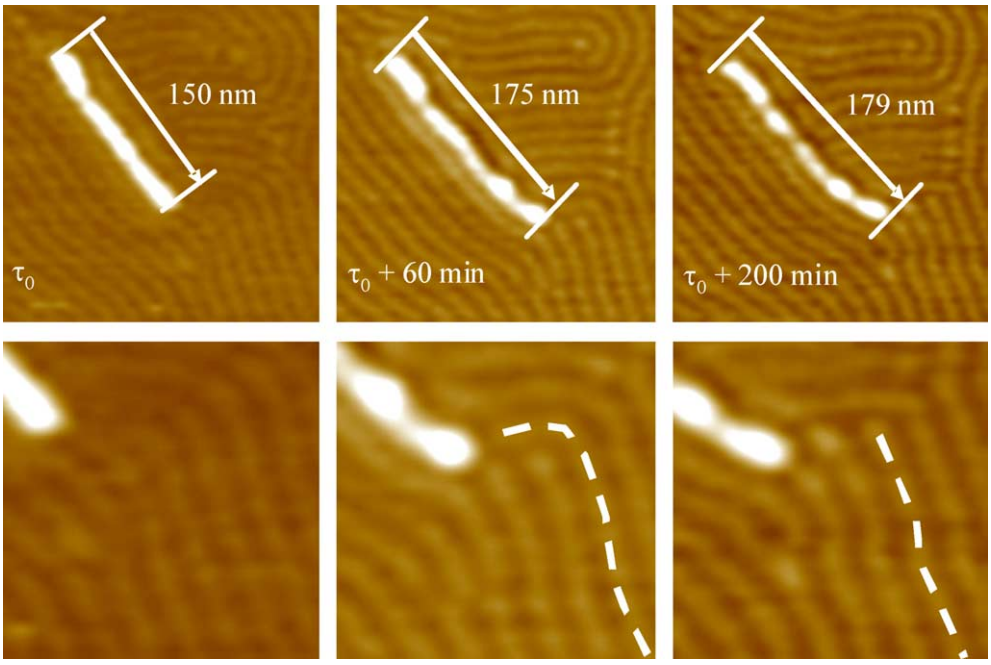

Fig. 4. AFM phase images of BEO 28 which show the temporal evolution of an isolated crystal and the surrounding mesophase at room temperature. The second and the third images of each row were captured 60 and 200 min after the first one, respectively. The images on the first row have a size of 500×500 nm^2. The images on the second row are the corresponding zooms to a size of 125×125 nm^2. Dashed lines are drawn to guide the eye.

chains implies changes in the conformations of the amorphous chains and rearrangements within the crystals. Such may happen already during crystallization but the most important rearrangements probably occur only after crystallisation in subsequent relaxations at room temperature. In particular for BEO 28, where the complete unfolding of the PEO stems will lead to significant stretching of the PB chains, such rearrangements are expected to become visible via changes in the morphology. We made a real-time AFM measurements of a chosen area (1×1 μm^2) containing only one isolated crystalline segment within a cylinder surrounded by a large amount of amorphous material in order to study the behaviour of the PEO crystals, and the corresponding changes in the PB matrix, at room temperature. We note that these crystals were, formed during a very short time (10 min) at relatively low temperature (−15 °C). In the chosen example, the average overall amount of crystallized material was only about 5%. The first interesting observation was that the crystal confined in the cylinder was still growing at room temperature. This was deduced from the length of the crystalline segment, which increased with time in the course of repeated imaging (Fig. 4). We followed the temporal and spatial evolution of the crystal and we found that the crystals are growing extremely slowly at room temperature—during a time-span of more than 3 h the length of the crystal increased only by 29 nm. However, the growth rate was not constant: during the first hour the crystal grew already by more than 20 nm. In Fig. 5, we show crystal length vs. time plots for three different crystals growing at room temperature in a cylindrical confinement. The plots clearly indicate a non-constant growth rate, also differing between samples. It is necessary to point out that despite the fact that the growth rate was not constant, it is clear that it was at maximum of the order of several tens of nanometers per hour, therefore much slower than the growth rate during the isothermal crystallization. Besides, and probably related to this observation, we detected also simultaneous changes in the morphology of the surrounding amorphous mesophase, namely straightening of some of the non-crystalline cylinders (shown by the white dashed line on Fig. 4) ahead of the growing crystal.

In an analogous experiment (the sample was again crystallized for 10 min at −15 °C and then measured at room temperature) we observed that crystal growth in two neighbouring cylinders or ‘tubes’ (laterally separated by about 100 nm, i.e. several tube diameters) proceeded at very

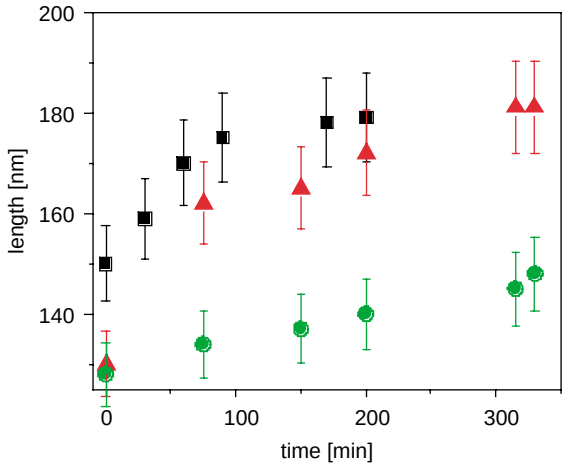

Fig. 5. Length vs. time plot for three isolated crystalline objects (squares correspond to the object shown in Fig. 4), measured on different samples and showing non-constant growth rate at room temperature.

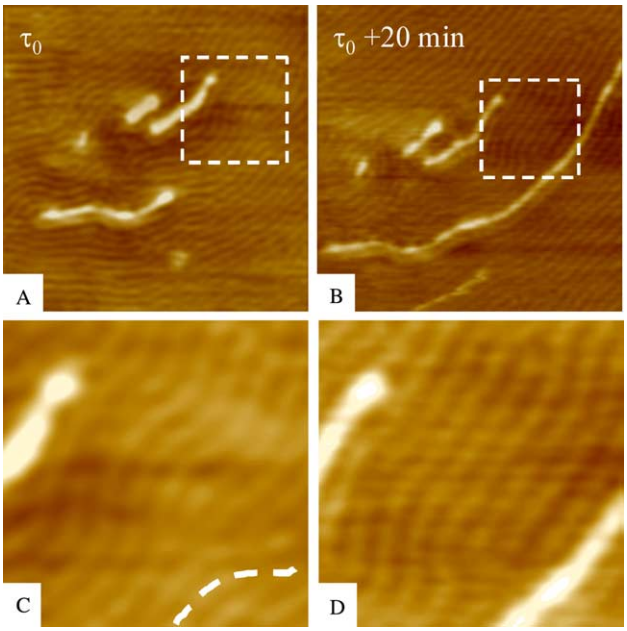

Fig. 6. AFM phase images of BEO 28 which show two neighbouring crystals growing at room temperature at different growth rates. The images (A) and (B) have a size of 500×500 nm^2 and the time interval is 20 min. The images (C) and (D) are the corresponding zoom-ins, indicated by dashed squares in (A) and (B), to a size of 165×165 nm^2. The dashed line in (C) is drawn to guide the eye and indicates the cylinder along which the 'fast' crystal is growing.

different growth rates (Fig. 6): while in one of the cylinders the crystal grew over more than 100 nm within 20 min, the length of the crystal in the other cylinder did not change within the lateral resolution of the AFM. In addition, the 'fast' growing crystal grew in a tube, which straightened during growth. Our observations on the changes in the amorphous mesophase in the proximity of the growth front (Figs. 4 and 6) indicate that the growing crystal can have an influence on the surrounding morphology—up to a few ten nanometers away from the growth front.

In many cases, we also observed that the crystals in the cylinders seemed to be interrupted, consisting of crystalline segments with lengths ranging from several nanometers up to a few tens of nanometers. These segments formed a 'pearl necklace'-like structure along the cylinder (Fig. 7). On the phase images shown in Fig. 7, the crystalline segments appear bright and are separated by darker zones along the cylinder. The darker zones may represent partially amorphous PEO regions or depletion zones where all PEO blocks were consumed, i.e. attached to the crystal. The reason for the formation of such zones is the fact that the PEO blocks are connected to long PB blocks, which prevent independent displacement of the PEO chains. Consequently, the PEO chains cannot move over large distances within the cylinder. In an attempt to explain the observed variation of the contrast along the cylinders seen in the AFM phase images, we propose a simple model of nucleation and crystal growth in a cylindrical mesophase. Once a nucleus is formed in the cylindrical compartment there is a feeding volume around it. Its size is defined by the mobility of the PEO chains. After the material in this volume is consumed (incorporated in the crystal), a depletion zone is formed which, in turn, causes a decrease of the growth rate. Thus, crystal growth along the cylinder cannot propagate at a constant velocity. In other words, in contrast to free PEO chains in a homopolymer thin film, in nanoscopic cylindrical domains of block copolymers crystal growth is even more frustrated, both by the confinement and by the limitations in displacement of the PEO chains. Within the cylinders, we assume that it is not sufficient to form one nucleus in order to allow for crystal growth along the whole length of the cylinder. Growth seems to be limited to a rather short range and has to be frequently 'restarted' by the formation of a new nucleus within this nanodomain. As a consequence, crystals grow at non-constant growth rate, depending strongly on the nucleation rate within the cylinder, which, in turn, may be also affected by defects (deviations in morphology or density) in the surrounding mesophase.

Complementary to above interpretation of the variation of the 'stiffness-contrast' along the cylinders seen in the AFM phase images, rearrangements within the crystalline zones may be relevant. During crystal growth at low temperatures around −20 °C, and thus at high growth rates, only rather imperfect crystal, but of homogenous structure along the cylinder, were formed. In the here presented AFM experiments, the samples were measured at room temperature where certainly some relaxations of the crystals occurred. As a consequence of such rearrangements within the crystals, domains of better order separated by less ordered domains or even depletion zones may have formed in this relaxation stage after growth. Here, such separation into less and better ordered domains may also be affected by the PB matrix. Less folded PEO chains impose also more highly stretched PB chains while less extended PB chains are attached to the folded PEO chains. A modulation of the degree of PEO chain folding along the cylinder may minimize

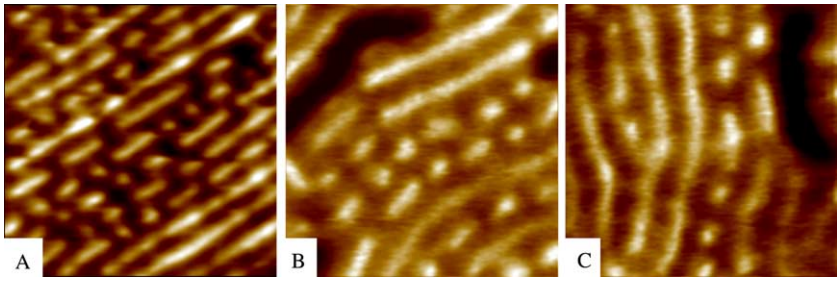

Fig. 7. AFM phase images of BEO 28 (A), BEO 25 (B) and cross-linked BEO 25 (C) showing that the crystalline PEO cylinders may consist of more perfect crystals (brighter objects) separated by less perfect crystals or even amorphous PEO. The size of the images is 250×250 nm^2.

the average stretching of the PB chains and thus be an alternative way to avoid the high entropy loss of highly stretched PB chains.

3.3. Templated and break-out crystallization

In order to perform our AFM measurements at ambient conditions the sample had to be transferred from the crystallization temperature T_c (~ -20 °C) to room temperature. This warming-up step represents a thermal annealing process which results in the tendency to form more perfect crystals in the cylinders, probably at the expense of material taken from the less perfect zones within the same cylinder. Obviously, such rearrangements can have a significant influence on the surrounding amorphous matrix (see Figs. 4 and 6). In the case of BEO 28 system, we even observe break-out crystallization (Fig. 8(B) and (C)), however, only at an intermediate range of the overall average amount X of the crystalline PEO cylinders in the sample. For X being less than 20% or higher than 70% we observed only templated crystallization. For X being in the range from 20 to 70%, we observed a combination of templated and break-out crystallization. Our explanation for how both types can be found in one sample is that break-out crystallization occurred only under certain conditions at later stages after templated isothermal crystallization confined to the cylinders took place. At early stages of the crystallization process, only a very small amount of PEO cylinders became crystalline. This small number of crystalline cylinders did not affect much the mesophase structure of the surrounding melt. The intrusion of growth fronts into the PB matrix is either prohibited or ineffective since the overall mechanical stress (related to the change in the inter-cylinder distance from about 16 to 22 nm, see Fig. 2) induced by the small number growing crystals cannot overcome the energetic barrier imposed by the PB matrix. This confining influence of the matrix results in templated crystallization. However, with the increase of the amount of crystalline PEO cylinders, i.e. with the corresponding increase of the overall mechanical stress, the perturbations in the melt structure become more and more pronounced. These perturbations can lead even to the destruction of the mesophase pattern and consecutively result in break-out crystallization. Interestingly, we never observed break-out crystallization on samples with high amount of crystallized PEO cylinders (70% and more). Probably, the crystallization rate was faster than the rate at which the mesophase pattern could respond to the perturbations.

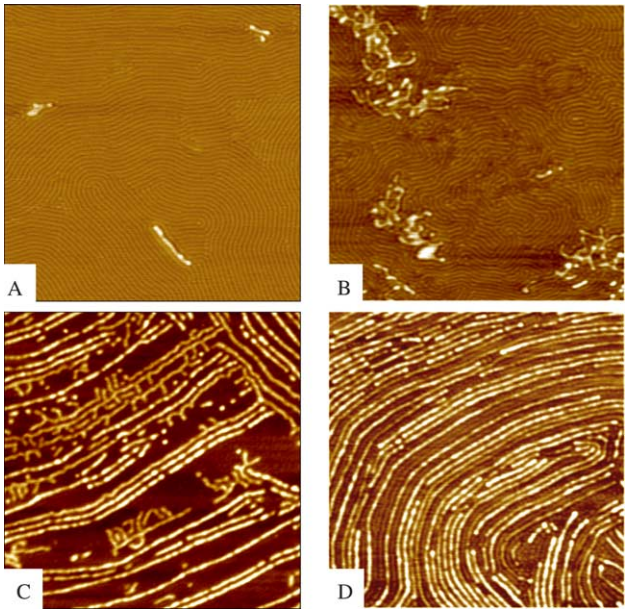

Fig. 8. AFM phase images of BEO 28, size is 1×1 μm^2. These samples are crystallized for different intervals of time at -17 °C: (A) -2 min, (B) -20 min, (C) -40 min and (D) -60 min. The average overall amount of crystallized PEO cylinders is about 5, 20, 60 and 80%, respectively.

In conclusion, our ex situ AFM measurements can help for the understanding of break-out crystallization. We have demonstrated that break-out crystallisation took only place in a second step, after the templated crystallization was slowed down or even stopped (e.g. by increasing the sample temperature. Such a temperature change occurred when the sample was mounted in the AFM). We note that with the rise of the sample temperature also the viscosity of the amorphous material decreased, hence the resistance of the PB matrix. This reduction in viscosity might allow for a more probable intrusion of the growing crystals into the PB matrix. In cases where most of the material was already crystallized at the time when we started to increase the sample temperature up to room temperature, there is not enough 'free space' to develop break-out crystallization. The remaining small amount of not yet crystallized material in the PEO domains did not allow for break-out crystallization. The small amount of amorphous PEO material is, so to say, 'locked in' by the predominant crystalline material. When the amount of the crystalline PEO domains was lower than about 20% (short crystallization periods) the intrusion of the growing crystals was not effective because the perturbations of the mesophase were not yet significant. When the amount of the crystallinity was higher than about 70% (after long crystallization periods) the growing crystals were too close to each other which resulted in preserving the mesophase pattern.

3.4. Kinetics of the increase of the amount crystalline material

Besides morphological aspects related to nucleation, crystallization and re-organisation processes at room temperature, we also studied in detail the kinetics of the increase of the amount of crystalline material in the samples—the evolution of the crystalline PEO domains with the time, for each of the polymers—BEO 28, BEO 25 and cross-linked BEO 25. In order to determine the amount of non-crystallized PEO material for each sample we used the method described already in the experimental part. In addition to the uncertainties in determining the crystallinity X arising from the analysis of the phase images, we could not exclude completely that some crystal growth took place also during the AFM measurements (at very low growth rates as it was shown before). Such growth would add up to a small systematic error in determining X. However, taking into account that the growth rate we measured

at room temperature (for templating crystallization) was only of the order of several tens of nanometers per hour, we can estimate the error due to relaxation and growth at room temperature to be smaller than the error bar of the method we used to quantify the amount of crystalline PEO domains. However, this may not be true for break-out crystallization since there crystal growth is not confined anymore and the crystallization rate should be considerably higher.

We plot, on semi-logarithmic scales, the amount of non-crystallized PEO cylinders (area fraction), as determined from the AFM images, vs. time for BEO 25. In Fig. 9(A), these results are compared with data from a related sample exhibiting spherical PEO domains in a PB matrix (BEO 17, data taken from Ref. [50]). The difference in the kinetics of the increase of the amount of crystalline material in cylindrical and spherical domains is clearly visible. In the case of BEO 17, the fraction n of non-crystalline PEO spheres could be approximated, at least for a large range, by:

$$n = n_{\infty}(1 - e^{-t/\tau}), \tag{3}$$

where n_{∞} and τ are the maximum fraction of crystallisable PEO spheres and the characteristic time constant of the crystallization process, respectively. This approach fits well the data points for early stages of crystallization. However, deviations from such a simple exponential behaviour were visible for the later stages. They could be attributed to the existence of some cells with a lower probability for crystallization [50].

It is important to note that for each system the crystallisation temperature T_c was chosen in such way that the crystallization rates of all three systems became comparable. The BEO 25 and BEO 17 samples were crystallized at −19 and −23 °C, respectively.

In case of BEO 25, the kinetics of the increase of the amount of crystalline material is more complex than proposed by Eq. (3). We observed two regimes of crystallization—at the early stages, crystalline material in BEO 25 sample increased comparatively slowly (the slope of the curve is smaller compared to the slope of the BEO 17 curve). A higher T_c of the BEO 25 system and the correspondingly lower nucleation rate may explain this difference. At the later stages, when crystallization in BEO 17 system started to 'slow down' (i.e. probability for nucleation decreased) for low amounts of non-crystallized spheres, the crystallization rate for BEO 25 became higher (despite higher T_c). After about 100 min the amount of crystallized PEO domains was higher for BEO 25 system compared to BEO 17 system. Such an increase in the overall crystallization rate for BEO 25 is probably due to the fact that for BEO 17 crystallinity is mostly controlled by the nucleation rate of the spherical domains, while in the cylindrical domains of BEO 25 we have in addition to the nucleation events also 'true' crystal growth along the cylinder, at least for some small distances.

In the case of BEO 28 we observed an intriguing 'jump' ('speeding up') of the crystallization rate at about 20% amount of crystalline PEO domains (Fig. 9(B)). As we have already

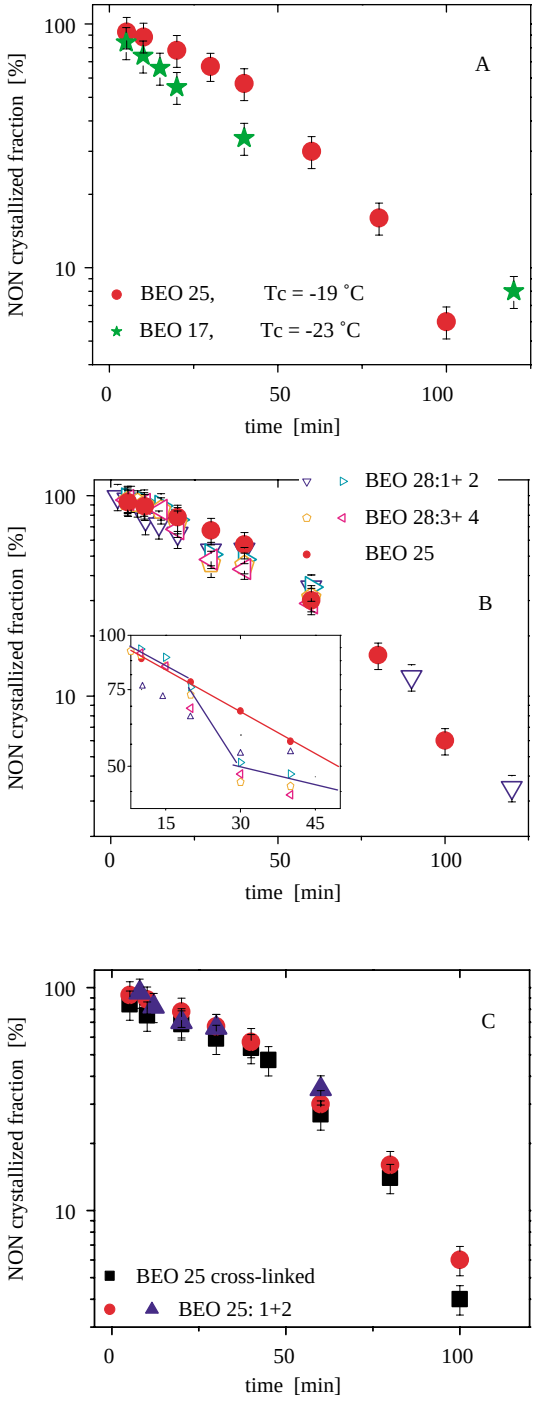

Fig. 9. (A) Amount of non-crystallized PEO domains as a function of the crystallization time for BEO 25 at −19 °C (circles) and for BEO 17 at −23 °C (stars: spherical PEO domains, data taken from Ref. [50]), (B) Four different series of measurements are shown for BEO 28 at −17 °C. They are compared with a BEO 25 curve measured at −19 °C. In the inset we show the 'jump' in the amount of crystalline domains caused by 'break-out', which occurs for BEO 28 at about 80% non-crystallized material. (C) Amount of non-crystallized PEO domains at −19 °C as a function of the time of crystallization for BEO 25 and cross-linked BEO 25.

mentioned above, BEO 28 samples with an overall average amount of crystallized PEO domains in the range 20–70% exhibited break-out crystallization. This jump-like increase in the amount of the crystallinity corresponds well to the

appearance of the break-out crystallization. If we disregard the range of 'the break-out jump' we obtained a similar rate in the variation in crystallinity before and after this range, which indicates that the 'jump' in crystallinity in the intermediate region is most likely due to growth events ('break-out') occurring after crystallisation at −17 °C.

Comparing the behaviour of cross-linked and non-cross-linked BEO 25 (Fig. 9(C)), we can conclude that in this particular system cross-linking has no observable influence on the crystallization rate. A small influence of cross-linking could, however, be hidden within the large scatter of the data, partially caused by the method we used to quantify the amount of the crystalline PEO domains.

4. Conclusions

In summary, we can conclude that in micro-phase separated asymmetric diblock copolymers crystallization occurs separately and independently in each compartment of the mesophase pattern. Due to the confined geometry of the PEO domains and large undercooling (high crystallization rate), the chains of the crystallisable block are trapped in various metastable states (i.e. folded crystalline chains) within these domains, which can result in crystals with different degree of perfection.

Growth rate within one single cylinder is not necessarily constant. It is possible that crystallisation within a cylinder starts or restarts from many nuclei along the cylinder and can be influenced by defects in the mesophase pattern, the molecular weight of the system and the interaction with the substrate.

Due to imperfections of the fast grown crystals, important rearrangements of the crystalline structure occur after crystallisation, leading to an increase of the internal degree of order of the crystalline PEO blocks, in particular at temperature higher than the crystallisation temperature and close to the melting point. Such rearrangements within the crystals can also lead to interruption of the crystals within the cylinders. Similar to the crystallisation process itself, such rearrangements within the crystals can also affect the amorphous matrix. Relaxations can even lead to changes in the mesophase morphology, which, in turn, can lead to break-out crystallization. Such was observed for the system of rather short blocks where crystallisation led to a change of the inter-cylinder spacing, i.e. the thickness of the crystalline PEO lamella was larger than the diameter of the molten PEO cylinders. The kinetics of the increase of the crystalline material reflects the possibility for break-out crystallisation in an intermediate crystallinity range. We did not find any indications for a destruction of the mesophase pattern at neither low nor high number of crystalline cylinders. Thus, we infer that at the low crystallisation temperatures the re-organisation of the mesophase morphology needed more time than the crystallisation process. Alternatively, at higher temperatures crystallisation is much slower than rearrangements of the mesophase. Noting that at any of the temperatures used in our experiments the PB matrix was above its glass transition temperature, we conclude that break-out crystallisation is a phenomenon depending on the crystallisation rate and not necessarily a phenomenon which occurs as soon as the matrix confining the cylindrical or spherical compartments becomes rubbery.

References

[1] Reiter G, Castelein G, Hoerner P, Riess G, Blumen A, Sommer J-U. Phys Rev Lett 1999;83:3844–7.
[2] Ryan AJ, Hamley IW, Bras W, Bates FS. Macromolecules 1995;28:3860–8.
[3] Loo Y-L, Register RA, Ryan AJ. Phys Rev Lett 2000;84:4120–3.
[4] De Rosa C, Park C, Thomas EL, Lotz B. Nature 2000;405:433–7.
[5] Loo Y-L, Register RA, Adamson DH. Macromolecules 2000;33:8361–6.
[6] Loo Y-L, Register RA, Adamson DH. J Polym Sci B 2000;38:2564–70.
[7] Chen H-L, Hsiao S-C, Lin T-L, Yamauchi K, Hasegawa H, Hashimoto T. Macromolecules 2001;34:671–4.
[8] Zhu L, Cheng SZD, Calhoun BH, Ge Q, Quirk RP, Thomas EL, et al. Polymer 2001;42:5829–39.
[9] Muthukumar M, Ober CK, Thomas EL. Science 1997;277:1225–32.
[10] Hamley IW. The physics of block copolymers. Oxford: Oxford University Press; 1998.
[11] Goldacker T, Abetz V, Stadler R, Erukhimovich Ya, Leibler L. Nature 1999;398:137–9.
[12] Jeong U, Kim H-C, Rodriguez RL, Tsai IY, Stafford CM, Kim JK, et al. Adv Mater 2002;14:274–6.
[13] Krausch G, Magerle R. Adv Mater 2002;14:1579–83.
[14] Ikkala O, Ten Brinke G. Science 2002;295:2407–9.
[15] Riess G. Prog Polym Sci 2003;28:1107–70.
[16] Cohen RE, Cheng PL, Douzinas K, Kofinas P, Berney CV. Macromolecules 1990;23:324.
[17] Douzinas KC, Cohen RE, Halasa AF. Macromolecules 1991;24:4457.
[18] Hamley IW, Fairclough JPA, Bates FS, Ryan AJ. Polymer 1998;39:1429.
[19] Khandpur AK, Macosko CW, Bates FS. J Polym Sci, Part B: Polym Phys 1995;33:247.
[20] Kofinas P, Cohen RE. Macromolecules 1994;27:3002.
[21] Sakurai K, MacKnight WJ, Lohse DJ, Schulz DN, Sissano JA, Lin JS, et al. Polymer 1996;37:4443.
[22] Quiram DJ, Register RA, Marchand GR, Adamson DH. Macromolecules 1998;31:4891.
[23] Rangarajan P, Haisch CF, Register RA, Adamson DH, Fetters LJ. Macromolecules 1997;30:494.
[24] Park C, De Rosa C, Fetters LJ, Thomas EL. Macromolecules 2000;33:7931.
[25] Gast AP, Vinson PK, Cogan-Farinas KA. Macromolecules 1993;26:1774.
[26] Gervais M, Gallot B. Makromol Chem 1973;174:193.
[27] Mai S, Fairclough JPA, Hamley IW, Matsen MW, Denny RC, Liao B, et al. Macromolecules 1997;30:8392.
[28] Ryan AJ, Hamley IW, Bras W, Bates FS. Macromolecules 1995;28:3860.
[29] Ryan AJ, Fairclough JPA, Hamley IW, Mai S, Booth C. Macromolecules 1997;30:1723.
[30] Zhu L, Cheng SZD, Calhoun BH, Ge Q, Quirk RP, Thomas EL, et al. J Am Chem Soc 2000;122:5957.
[31] Zhu L, Chen Y, Zhang A, Calhoun BH, Chun M, Quirk RP, et al. Phys Rev B 1999;60:10022.
[32] Nojima S, Kato K, Yamamoto S, Ashida T. Macromolecules 1992;25:2237.
[33] Ishikawa S, Ishizu K, Fukutomi T. Eur Polym J 1992;28:1219.
[34] Liu L-Z, Yeh F, Chu B. Macromolecules 1996;29:5336.
[35] Lotz B, Kovacs AJ. Kolloid ZZ Polym 1966;209:97.
[36] Lotz B, Kovacs AJ, Bassett GA, Keller A. Kolloid ZZ Polym 1966;209:115.
[37] Hamley IW, Wallwork ML, Smith DA, Fairclough JPA, Ryan AJ, Ma S-M, et al. Polymer 1998;39:3321.
[38] Xu J-T, Turner SC, Fairclough JPA, Mai S-M, Ryan AJ, Chaibundit C, et al. Macromolecules 2002;35(9):3614–21.

[39] Xu J-T, Fairclough JPA, Mai S-M, Ryan AJ, Chaibundit C. Macromolecules 2002;35(18):6937–45.
[40] Loo Y-L, Register RA, Ryan AJ, Dee GT. Macromolecules 2001;34(26):8968–77.
[41] Loo Y-L, Register RA, Ryan AJ. Macromolecules 2002;35(6):2365–74.
[42] Schmalz H, Müller AJ, Abetz V. Macromol Chem Phys 2003;204:111–24.
[43] Albuerne J, Márquez A, Müller AJ, Raquez J, Degée Ph, Dubois Ph, et al. Macromolecules 2003;36:1633–44.
[44] Müller AJ, Arnal M, Spinelli AL, Cañizales E, Puig C, Wang H, et al. Macromol Chem Phys 2003;204:1497–513.
[45] Zhu L, Cheng SZD, Calhoun BH, Ge Q, Quirk RP, Thomas EL, et al. J Am Chem Soc 2000;122(25):5957–67.
[46] Huang P, Zhu L, Guo Y, Ge Q, Jing AJ, Chen WY, et al. Macromolecules 2004;37(10):3689–98.
[47] Reiter G, Castelein G, Sommer J-U, Röttele A, Thurn-Albrecht T. Phys Rev Lett 2001;86:5918.
[48] Massa MV, Carvalho JL, Dalnoki-Veress K. Eur Phys JE 2003;12:111–7.
[49] Taden A, Landfester K. Macromolecules 2003;36:4037–41.
[50] Röttele A, Thurn-Albrecht T, Sommer J-U, Reiter G. Macromolecules 2003;36(4):1257–60.
[51] Schmalz H, Knoll A, Müller AJ, Abetz V. Macromolecules 2002;35:10004–13.
[52] Muller AJ, Balsamo V, Arnal ML, Jakob T, Schmalz H, Abetz V. Macromolecules 2002;35(8):3048–58.
[53] Müller AJ, Arnal ML, López-Carrasquero F. Macromol Symp 2002;183:199–204.
[54] Schmalz H, Abetz V, Müller AJ. Macromol Symp 2002;183:179–84.
[55] Kelton KF. In: Ehrenreich H, Turnbull D, editors. Crystal nucleation in liquids and glasses, vol. 45. Boston: Academic Press; 1991.
[56] Semenov AN. JETP 1985;61:733–42.
[57] Knoll A, Magerle R, Krausch G. Macromolecules 2001;34:4159.
[58] Vasilev C, Heinzelmann H, Reiter G. J Polym Sci, Part B 2004;42:1312–20.
[59] Due to the finite size and the shape of the probe tip the lateral resolution of the AFM is limited—in case of measuring features with lateral size comparable to the radius of curvature of the tip, the AFM image will be dominated by the shape of the tip.